Available online at www.sciencedirect.com
SCIENCE DIRECT
Journal of Sound and Vibration 296 (2006) 406–415
JOURNAL OF SOUND AND VIBRATION
www.elsevier.com/locate/jsvi

Short Communication

A forward-advancing wave expansion method for numerical solution of large-scale sound propagation problems

L. Barrera Rolla*, H.J. Rice

Department of Mechanical and Manufacturing Engineering, Trinity College, Dublin 2, Ireland

Received 10 March 2005; received in revised form 24 February 2006; accepted 27 February 2006
Available online 23 May 2006

Abstract

In this paper a "forward-advancing" field discretization method suitable for solving the Helmholtz equation in large-scale problems is proposed. The forward wave expansion method (FWEM) is derived from a highly efficient discretization procedure based on interpolation of wave functions known as the wave expansion method (WEM). The FWEM computes the propagated sound field by means of an exclusively forward advancing solution, neglecting the backscattered field. It is thus analogous to methods such as the (one way) parabolic equation method (PEM) (usually discretized using standard finite difference or finite element methods). These techniques do not require the inversion of large system matrices and thus enable the solution of large-scale acoustic problems where backscatter is not of interest. Calculations using FWEM are presented for two propagation problems and comparisons to data computed with analytical and theoretical solutions and show this forward approximation to be highly accurate. Examples of sound propagation over a screen in upwind and downwind refracting atmospheric conditions at low nodal spacings (0.2 per wavelength in the propagation direction) are also included to demonstrate the flexibility and efficiency of the method.

1. Introduction

The wave expansion method (WEM) [1–5] is a very flexible, efficient full field method for solving the Helmholtz equation, which can model complicated ground topography, ground impedance inhomogeneities and inhomogeneous moving media. Although, WEM interpolation gives accurate results with a mesh spacing of less than three points per wavelength, when dealing with extensive domains, the computational resources will eventually become prohibitive.

A possible answer to sound scattering in large-scale acoustical problems is to consider only the sound waves travelling in one direction as this will remove the need for full system matrix inversion. This has been proposed, for example, using the parabolic equation method (PEM) [6–9]. Using the forward wave expansion method (FWEM) in a similar way, backscattered waves are ignored which permits a computationally light forward advancing solution to be formulated whilst retaining the other formulation advantages of WEM.

*Corresponding author.
E-mail address: barrerl@tcd.ie (L.B. Rolla).

0022-460X/$ - see front matter © 2006 Elsevier Ltd. All rights reserved.
doi:10.1016/j.jsv.2006.02.023

2. Implementation

To compute the sound pressure distribution of the domain shown in Fig. 1a with FWEM, a "local mesh" is formed by using a few "columns" of nodes (see Fig. 1b). Three was the minimum number of columns used for the calculations presented in this study. If the solution is advancing to the right, a free radiating condition is imposed on the right-hand side of the local mesh. In addition to the high discretization efficiency, the WEM method also has a natural and robust radiation condition [5] which makes it suitable for this type of formulation.

Neumann, impedance or radiation boundary conditions are applied to the upper and lower faces as required by the model. A Dirichlet condition using precalculated values is imposed on the left of the subdomain (except in the case of the first local domain). Once the sound pressure is calculated for the subdomain, the solution may be advanced in space. Fig. 2 shows the restraint scheme applicable to each local mesh.

The implementation of the general wave discretization method utilized within each subdomain now follows the standard WEM formulations. For each point $\mathbf{r}_0$ in the subdomain, the pressure can be approximated by the superposition of N plane waves of strength γ_n:

$$p_{(\mathbf{r}_0)} = \sum_{n=1}^{N} \gamma_n e^{-jk(\mathbf{d}_n \cdot \mathbf{r}_0)}, \tag{1}$$

where $\mathbf{d}_n$ is the unit propagation direction vector of the nth plane wave and k is the wavenumber. In the original WEM the complete range of directions $[0, 2\pi]$ are used. In FWEM, as only forward propagation is being considered the range is restricted to $[-\pi/4, \pi/4]$. This selection tolerates a nodal spacing of less than three per wavelength. As the calculation proceeds to field positions more remote from the source, this angular spread may be reduced. This permits use of lower nodal spacings in the propagation direction.

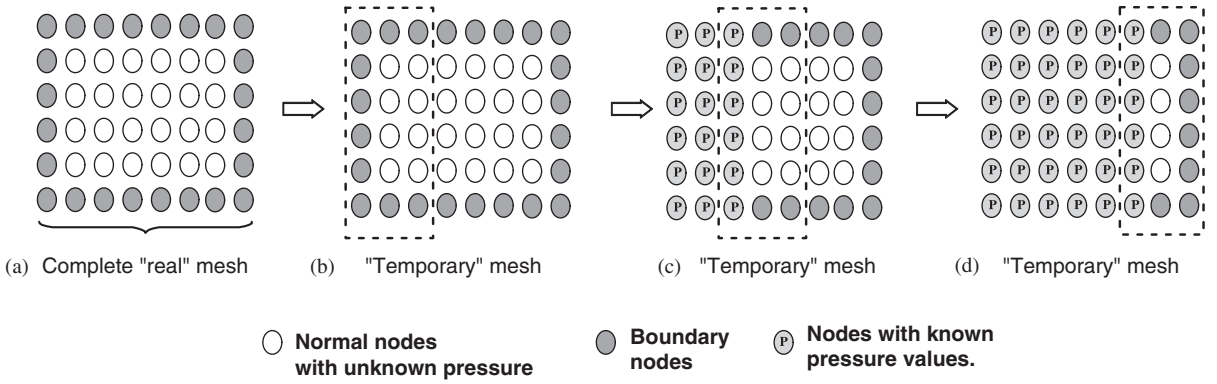

Fig. 1. Domain representation.

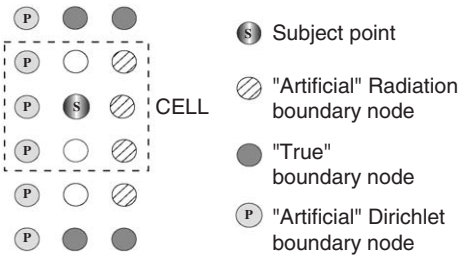

Fig. 2. Forward WEM cells.

Using matrix notation, Eq. (1) may be written as

$$p_{(\mathbf{r}_0)} = \mathbf{h}_{(\mathbf{r}_0)} \cdot \mathbf{g}, \tag{2}$$

where $\mathbf{h}_{(\mathbf{r}_0)}$ is a $1 \times N$ row vector of plane waves functions evaluated at $\mathbf{r}_0$ and $\mathbf{g}$ is a column vector of the wave strengths, γ_n.

If the same approximation is applied to the other nodal positions in the cell we can write

$$\mathbf{p} = \mathbf{H} \cdot \mathbf{g}, \tag{3}$$

where $\mathbf{p}$ is a $M \times 1$ vector of the pressures at each surrounding node $\mathbf{r}_m$, $1 \leqslant m \leqslant M$, and

$$\mathbf{H}_{mn} = \mathrm{e}^{-jk(\mathbf{d}_n \cdot \mathbf{r}_m)}.$$

A computational template may then be formed by combining Eqs. (2) and (3) to give

$$p_{(\mathbf{r}_0)} = \mathbf{h}_{(\mathbf{r}_0)} \mathbf{H}^{+} \mathbf{p}, \tag{4}$$

where the $\mathbf{H}^{+}$ is a pseudo-inverse of matrix $\mathbf{H}$.

Eq. (4) is referred to as the wave expansion discretization (WED) method and is similar to the fundamental formulation commonly referred to as GFD which uses Greens functions rather than plane waves as basis functions [1,2]. The template from Eq. (4) may be then used to form individual rows of the system's dynamic stiffness matrix.

2.1. Dirichlet boundary condition

For points lying adjacent to a boundary with Dirichlet boundary condition, this boundary condition is directly implemented constraining the appropriate degrees of freedom in the assembled stiffness matrix.

2.2. Neumann boundary condition

If the subject point, $\mathbf{r}_0$, is part of a boundary with outward normal $\mathbf{n}_0$ and Neumann boundary conditions given by

$$\frac{\partial p_{(\mathbf{r}_0)}}{\partial \mathbf{n}_0} = q_0, \tag{5}$$

the constraint Eq. (3) may be directly augmented to

$$\begin{Bmatrix} \mathbf{p} \\ q_0 \end{Bmatrix} = \begin{bmatrix} \mathbf{H} \\ \partial h_{(\mathbf{r}_0)} / \partial \mathbf{n}_0 \end{bmatrix} \cdot \mathbf{g} = \mathbf{H}_{\mathtt{aug}} \cdot \mathbf{g}. \tag{6}$$

Applying the pseudo-inversion to $\mathbf{H}_{\mathtt{aug}}$, substituting and left–right partitioning the resulting equation, the reformulation expression of Eq. (2) then yields

$$p_{(\mathbf{r}_0)} = \mathbf{h}_{(\mathbf{r}_0)} (\mathbf{H}^{+}_{\mathtt{aug}})_L \mathbf{p} + \mathbf{h}_{(\mathbf{r}_0)} (\mathbf{H}^{+}_{\mathtt{aug}})_R \mathbf{q}. \tag{7}$$

2.3. Impedance boundary condition

Impedance boundary condition implementation follows a similar procedure as the one described above. If the condition for point $\mathbf{r}_0$, is given by

$$\frac{\partial p_{(\mathbf{r}_0)}}{\partial \mathbf{n}} = -j \frac{\rho_0 w}{Z} p_{(\mathbf{r}_0)}, \tag{8}$$

where $\mathbf{r}_0$ is any point laying on the boundary with impedance condition, $\mathbf{n}$ is the radiating normal outward boundary, w is the angular frequency, Z is the specific acoustic impedance of the surface at that point, and ρ_0 is the air density.

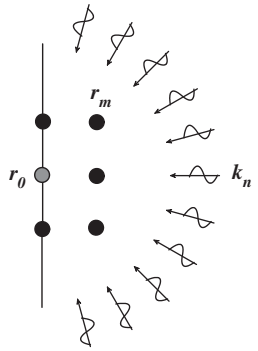

Fig. 3. "Natural" radiation boundary condition implementation.

Eq. (3) is then augmented to

$$\left\{ \begin{matrix} \mathbf{p} \\ 0 \end{matrix} \right\} = \left[\begin{matrix} \mathbf{H} \\ \partial h_{(\mathbf{r}_0)}/\partial \mathbf{n}_0 + j(\rho_0 w/Z) h_{(\mathbf{r}_0)} \end{matrix} \right] \cdot \mathbf{g} = \mathbf{H}_{\mathtt{aug}} \cdot \mathbf{g}. \tag{9}$$

After pseudo-inversion and partitioning, the template reduces to

$$p_{(\mathbf{r}_0)} = \mathbf{h}_{(\mathbf{r}_0)} (\mathbf{H}^{+}_{\mathtt{aug}})_L \mathbf{p}.$$

2.4. Natural radiation boundary condition

A simple method to implement a natural radiation boundary condition [5] is to restrict the propagation directions of the fundamental basis solutions to a selection of those propagating outwards from the computational domain, as shown in Fig. 3.

A special radiating template equation may then be constructed,

$$\mathbf{p} = \mathbf{H}_{\mathtt{rad}} \cdot \mathbf{g}$$

and the template for the radiation point given by

$$p_{(\mathbf{r}_0)} = \mathbf{h}_{(\mathbf{r}_0)} \mathbf{H}^{+}_{\mathtt{rad}} \mathbf{p}. \tag{10}$$

Once the subdomain is assembled and the "new" boundary conditions (true and "artificial") are applied, the local equation system can be solved for acoustic pressure at these nodes. A neighbouring subdomain can then be formulated and the solution advanced.

3. Specific modelling issues

3.1. Source modelling and near field computation

As in the PEM, the FWEM will present some problems in modelling the sound sources and computing the pressure values in regions near sources or in locations where the curvature of the sound field is high. Results show that the pressure values obtained in the acoustic field remote from these will not be influenced significantly by these local inaccuracies.

3.2. Upper attenuating boundary layer

To reduce spurious reflections from the upper boundary back into the computational domain, additional treatment of the radiation boundary condition may be applied by introducing an artificial absorbing boundary

layer. In this layer, an artificial attenuation is gradually increased with height, starting with zero attenuation at $z = z_t$ (where z_t is the height of the bottom of the absorbing layer). This attenuation is achieved by adding an imaginary term to the wavenumber $k(z)$ according to [8],

$$k = k_0 - jA[(z - z_t)/(z_M - z_t)]^2, \tag{11}$$

where k_0 is the wavenumber in the operational part of the domain, A is a constant, and z_M is the z coordinate of the top boundary.

The introduced damping should not be too large as this will produce reflections back into the lower part of the atmosphere although it is not clear how to optimize this in the present context.

4. Numerical results

The advancing method was tested for two different benchmark problems, a free radiation problem and a simple edge diffraction problem. In both cases the ground was considered to be perfectly reflecting ($\partial P/\partial \mathbf{n} = 0$). Results were compared with theoretical solutions, Hankel functions (for free radiation problems) and a Fresnel Integration [13] approximation for the diffraction problems. The diffraction problem was also compared with approximate results obtained with the ISO9613-2 [12] formulation. Two examples of diffraction of sound over a barrier in a refracting atmosphere are also included to demonstrate the flexibility of the method.

4.1. Free field propagation

The geometry of the first problem is shown in Fig. 4.

The source was positioned at point $(x, y) = (0, 0)$. The operating frequency was 1000 Hz. The domain was 1 km long, 50 m height, and 5,012,505 nodes were used in the model which gave a nodal spacing of three nodes per wavelength. An absorbing layer $50 \times \lambda$ deep was applied. This set-up leaves an operational altitude of 30 m. The absorbing layer was formulated using the model in expression (11) with constant $A = 0.9$. The effect of the absorbing layer can be seen in Fig. 5.

The resulting field in the operational part of the domain is shown in Fig. 6.

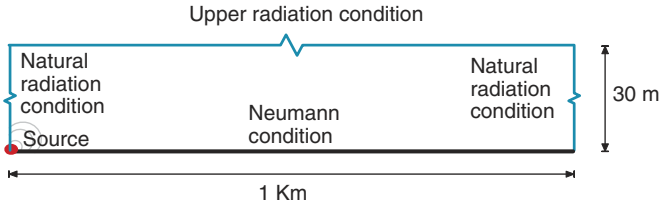

Fig. 4. Geometry of the problem.

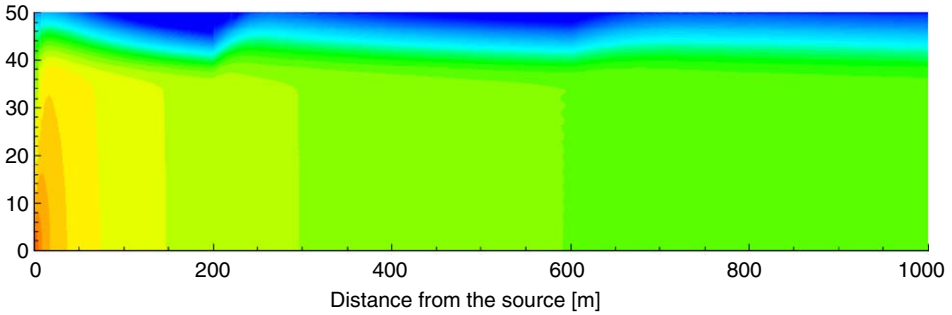

Fig. 5. FWEM, sound pressure level (dB).

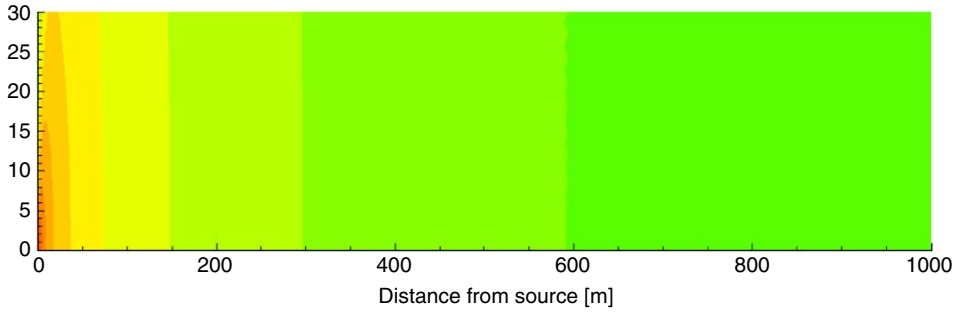

Fig. 6. FWEM, sound pressure level (dB). Operational part.

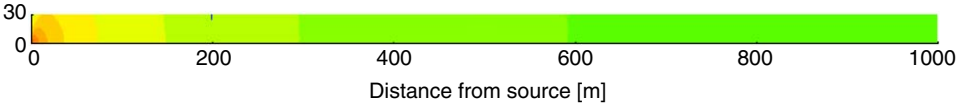

Fig. 7. True vertical–horizontal scale plot.

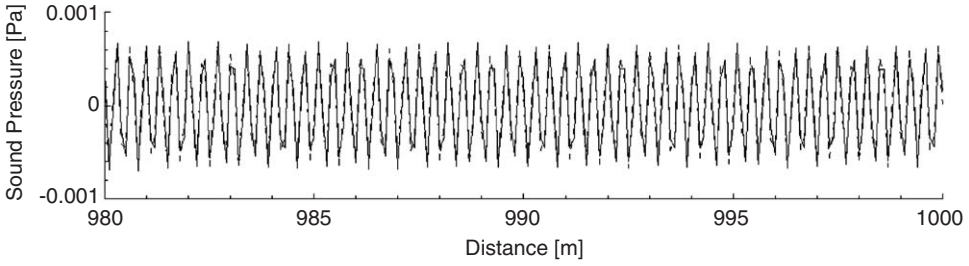

Fig. 8. Real part of the pressure values in the last 10 m (Pa), at a line 2 m above the ground level. — FWEM, - - theoretical solution (Hankel function).

Fig. 7 shows the true vertical–horizontal scale. This shows that the problem has extremely shallow grazing angles on the upper boundary of the domain. This may be compared to the free field radiation computed using the following Hankel function:

$$P_{\text{theoretical}} = -\frac{j}{4} H_0^{(2)}(k\mathbf{r}).$$

A plot of the real part of the sound pressure values obtained with the FWEM and the analytic solution for the last 20 m of the domain at an elevation 2 m above ground level is given in Fig. 8.

A plot of the sound pressure level (SPL) of the sound pressure values obtained with the FWEM and the analytic solution at an elevation 2 m above ground level is given in Fig. 9.

4.2. *Diffraction by a sound barrier*

The second geometry studied is shown in Fig. 10.

The source was positioned at point $(x, y) = (0, 0)$. The operating frequency was 1000 Hz. The domain was 1 km long and 5,012,425 nodes were used which gave a nodal density of three per wavelength. The top 20 m were changed into an absorbing layer whilst a loss free domain of height 30 m was maintained. The absorbing layer was formulated using the model in Eq. (11) with constant $A = 0.9$. Fig. 11 shows the results for the first 100 m of the domain.

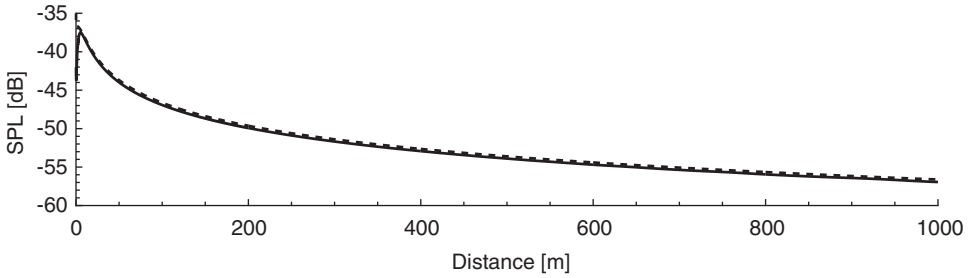

Fig. 9. SPL (dB), at a line 2 m above the ground level. — FWEM, - - theoretical solution (Hankel function).

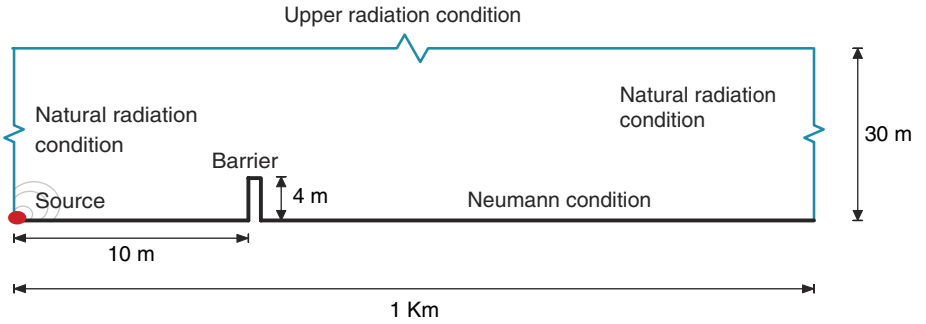

Fig. 10. Geometry of the problem.

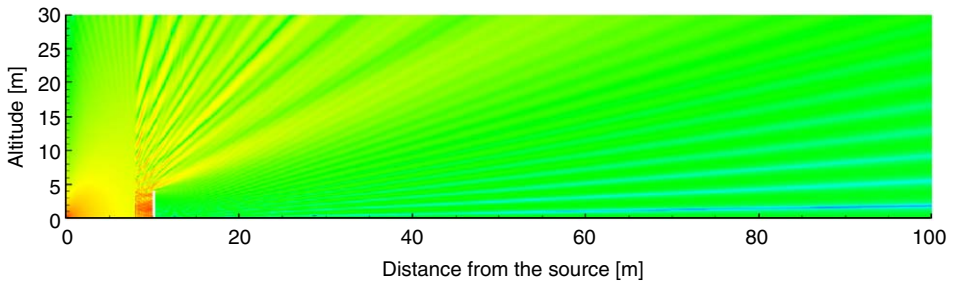

Fig. 11. FWEM, sound pressure level (dB) for the first 100 m.

The resulting sound field for the complete domain is shown in Fig. 12.

The insertion loss was computed in a line at ground level and compared with results obtained with the ISO9613-2 [12] and a Fresnel integral method [13,14]. The results are shown in Fig. 13.

This figures show the accuracy of the method.

4.3. *Diffraction by a sound barrier in a refracting atmosphere*

For the following examples which demonstrate the flexibility and efficiency of the method, the same geometry of Section 4.2 is used. A logarithmic sound speed profile was introduced to model the refraction [9–11]:

$$c_{(z)} = \begin{cases} c_0 + b \cdot \ln\left(\dfrac{z}{z_0}\right) & \text{for } z \geqslant z_0, \\ c_0 & \text{for } z \leqslant z_0, \end{cases}$$

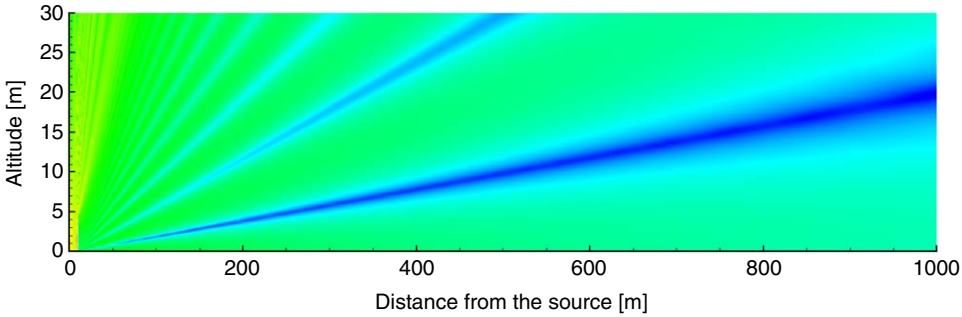

Fig. 12. FWEM, sound pressure level (dB). Operational part.

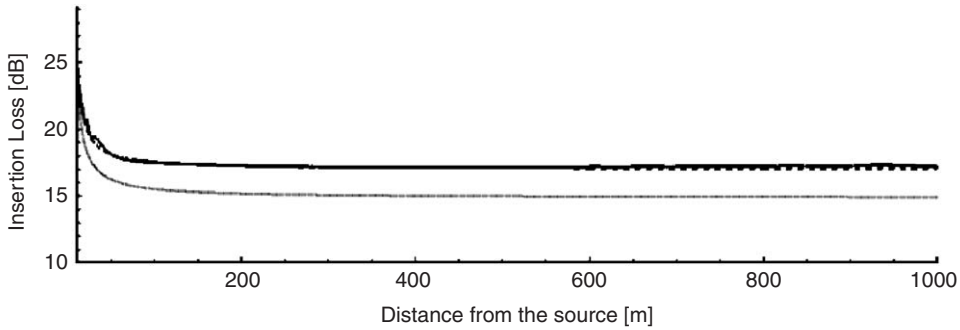

Fig. 13. Insertion loss (dB). — FWEM, — ISO9613-2, - - Fresnel method.

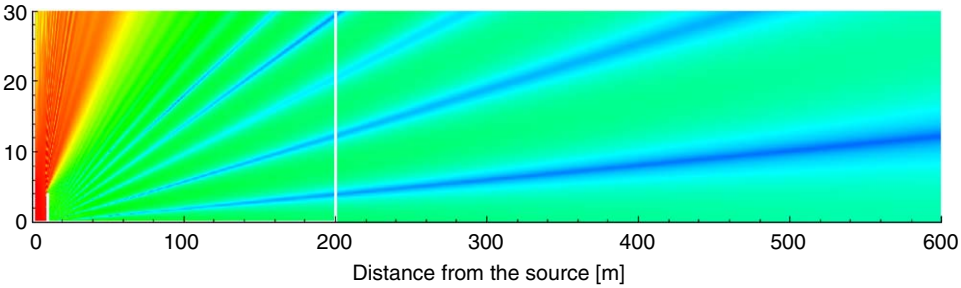

Fig. 14. FWEM, sound pressure level (dB). Non-refracting atmosphere.

where z_0 is 0.1 m for this example, and b is a parameter that can be positive or negative. For downwind refraction b is positive and for upwind directions b is negative. This was directly implemented by allowing the wavenumber k to vary accordingly through the field. In addition, the angular spread of propagation directions to right of the position marked 200 m was reduced to $[-\pi/12, \pi/12]$. This allows the nodal spacing to be increased to 0.2 nodes per wavelength in the propagation direction.

Fig. 14 shows the resulting sound field for a non-refracting atmosphere. Figs. 15 and 16 show the resulting sound fields for a downwind and an upwind refracting atmosphere, respectively.

It should be noted that the previous examples are included only to demonstrate the flexibility of the method. The logarithmical sound speed profile used in these examples do not take into account additional wind speed gradients induced by the screen. These screen induced wind-speed gradients enhance the downward refraction of sound waves [16]. More realistic sound speed profiles can be introduced into the model in a similar way.

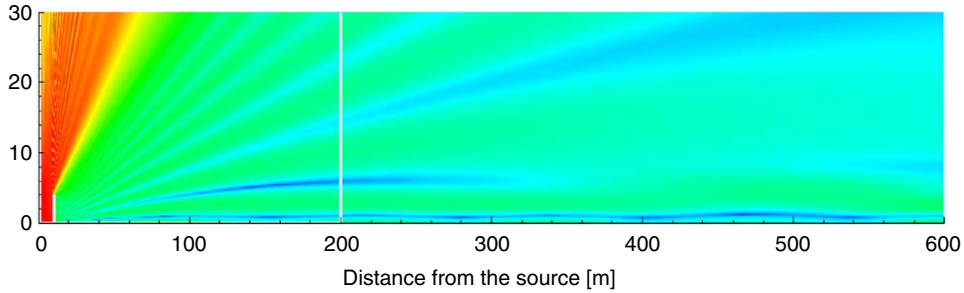

Fig. 15. FWEM, sound pressure level (dB). Downwind refracting atmosphere.

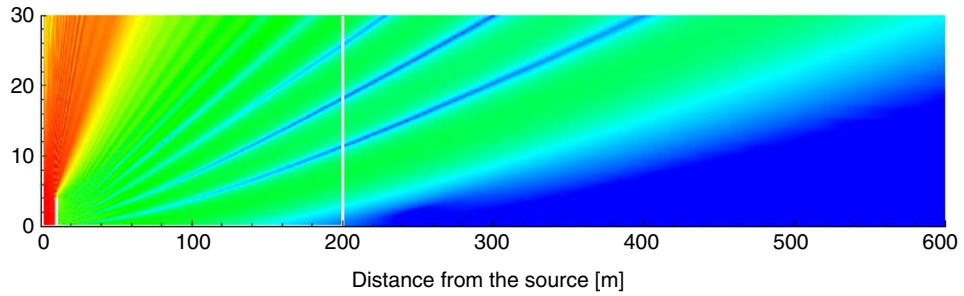

Fig. 16. FWEM, sound pressure level (dB). Upwind refracting atmosphere.

5. Discussion

It can be seen from the results that the FWEM offers the basis of a highly accurate discretization method to solve the Helmholtz equation for extensive domains with low mesh densities.

As expected, due to loss of reflections from obstacles and difficulties modelling wave fronts with high curvature, the FWEM gives unreliable results in the near field. This problem can be circumvented to some extent by using the regular WEM for the near field calculations and including a large number of columns in the calculation of the starter field. The radiation condition used on the advancing front is adequate once the wave front angles are not too oblique. The treatment of upper radiation condition is critical but this is a problem with any acoustic calculation in a field with shallow grazing angles and is not specific to this method. It should be noted that even a combination of an absorbing layer and a radiation condition cannot *completely* eliminate spurious reflections.

Examples of sound propagation over a sound barrier in a refractive atmosphere where the wavenumber is allowed to vary within the field demonstrate the intrinsic flexibility of the method.

Although only regular meshes have been used in the calculations presented in this paper, FWEM may also be formulated using irregular meshes thus enabling modelling around objects of arbitrary shape. An example of sound propagation over a wedge shaped object is shown in Ref. [15]. An issue which will now arise is the identification of the advancing front.

If regular meshes are used and there are no wavenumber parameter changes across a computational front then the advancing method may be made completely explicit.

When the wavefronts become more planar in nature the formulation may be adjusted by restricting the range of propagation directions of the basis functions. This will allow further reduction of the mesh density in the propagation direction. In this paper examples are included with a nodal spacing of 0.2.

Acknowledgements

The authors gratefully acknowledge the funding provided by the Irish Higher Education Authority programme-PRTLi cycle 3-TRIP.

References

[1] J.E. Caruthers, J.C. French, G.K. Raviprakash, Recent developments concerning a new discretization method for the Helmholtz equation, *First AIAA/CEAS Aeroacoustics Conference*, *CEAS/AIAA-95-117*, Munich, Germany, 1995, pp. 819–826.

[2] J.E. Caruthers, J.C. French, G.K. Raviprakash, Green function discretization for numerical solution of the Helmholtz equation, *Journal of Sound and Vibration* 187 (4) (1995) 553–568.

[3] G. Ruiz, Numerical Vibro/acoustic Analysis at Higher Frequencies, PhD Thesis, University of Dublin, 2002.

[4] J.E. Caruthers, R.C. Engels, G.K. Raviprakash, A wave expansion computational method for discrete frequency acoustics within inhomogeneous flows, *Second AIAA/CEAS Aeroacoustics Conference*, *CEAS/AIAA-96-1684*, State College, PA, May 1996, pp. 1–11.

[5] G. Ruiz, H.J. Rice, An implementation of a wave based finite difference scheme for a 3D acoustic problem, *Journal of Sound and Vibration* 256 (2) (2002) 373–381.

[6] M. West, K. Gilbert, R.A. Sack, A tutorial on the parabolic equation (PE) model used for long range sound propagation in the atmosphere, *Applied Acoustics* 37 (1992) 31–49.

[7] J.F. Claerbout, *Fundamentals of geophysical data processing, Initial-Value Problems in Two and Three dimensions*. International Series in the Earth and Planetary Sciences, McGraw-Hill, New York, USA, 1976.

[8] E.M. Salomons, Diffraction by a screen in downwind sound propagation: a parabolic equation approach, *Journal of Acoustical Society of America* 95 (6) (1994) 3109–3117.

[9] K.E. Gilbert, M.J. White, Application of the parabolic equation to sound propagation in a refracting atmosphere, *Journal of Acoustical Society of America* 85 (2) (1989) 630–637.

[10] K.E. Gilbert, M.J. White, Application of the parabolic equation to the outdoor propagation of sound, *Applied Acoustics* 27 (1989) 227–238.

[11] E.M. Salomons, Improved Green's function parabolic equation method for atmospheric sound propagation, *Journal of Acoustical Society of America* 104 (1) (1998) 100–111.

[12] International Organization for Standardization ISO 9613-2, Acoustics—Attenuation of Sound During Propagation Outdoors—part 2: General Method of Calculation, 1996.

[13] D.T. Blackstock, *Fundamentals of Physical Acoustics, Chapter 14—Diffraction*, Wiley-Interscience, New York, 2000.

[14] A.D. Pierce, *Acoustics. An Introduction to its Physical Principles and Applications, Chapter 5—Radiation From Sources Near and on Solid Surfaces*, Acoustical Society of America, New York, 1989.

[15] L. Barrera Rolla, H.J. Rice, Explicit Forward-Advancing Wave Expansion Method for Numerical Solution of Large Scale Sound Propagation Problems, ISMA2004, Leuven, 2004, pp. 1433–1448.

[16] E.M. Salomons, Reduction of the performance of a noise screen due to screen-induced wind-speed gradients. Numerical computations and wind-tunnel experiments, *Journal of Acoustical Society of America* 105 (4) (1999) 2287–2293.